

Chaotic fluctuations in a universal set of transmon qubit gates

Daniel Basilewitsch,¹ Simon-Dominik Börner,² Christoph Berke,²
Alexander Altland,² Simon Trebst,² and Christiane P. Koch^{1,*}

¹*Dahlem Center for Complex Quantum Systems and Fachbereich Physik, Freie Universität Berlin, D-14195 Berlin, Germany*

²*Institute for Theoretical Physics, University of Cologne, D-50937 Cologne, Germany*

(Dated: January 24, 2024)

Transmon qubits arise from the quantization of nonlinear resonators, systems that are prone to the buildup of strong, possibly chaotic, fluctuations. Such instabilities will likely affect fast gate operations which involve the transient population of higher excited states outside the computational subspace. Here we show that a statistical analysis of the instantaneous eigenphases of the time evolution operator, in particular of their curvatures, allows for identifying the subspace affected by chaotic fluctuations. Our analysis shows that fast entangling gates, operating at speeds close to the so-called quantum speed limit, contain transient regimes where the dynamics indeed becomes partially chaotic for just two transmons.

Introduction In coupled superconducting circuits, one of the leading platforms in quantum information science [1, 2], the nonlinearity of Josephson junctions serves to separate an energetically low-lying qubit subspace from a higher-lying state space whose presence has become a focus of attention [3–5]. The restriction to the computational subspace rests on the assumption that the energy stored in the initial state remains decentralized, and higher excited states of individual ‘qubits’ are not accessed. However, residual qubit-qubit couplings can be made algebraically, but never exponentially, small in the detuning from the resonator frequencies. Indeed, the presence of the higher-lying state space may be detrimental for stationary states relevant to storage of information, in particular so for fixed-frequency architectures [3]. While, for information storage, tunable couplers present one route to alleviate signatures of non-integrability, the issue of instabilities due to the non-linearity becomes all the more pressing for the implementation of gates.

Indeed, the population of energy levels outside of the computational subspace is rather common when implementing fast gates [6] or resetting superconducting qubits [7]. Fast device operation is desirable in view of optimal clock speeds but also to combat decoherence. The shortest possible time in which a given task can be carried out is referred to as the quantum speed limit (QSL) [8]. The QSL for quantum gates is fundamentally determined by the size of the effective time-dependent qubit-qubit couplings which are needed to generate entanglement — or, in the case of local rotation gates, to undo undesired entanglement due to residual couplings. Operation at the QSL is enabled by suitably tailored pulses which bring the population of higher lying levels during the gate operation back to the computational subspace at the end of the gate [9]. The corresponding time evolution, under the perspective of (classical) nonlinear dynamics, takes, however, place in a twilight zone between integrable dynamics in the limit of weak inter-transmon coupling and possibly chaotic fluctuations at larger couplings [4, 5]. Quantum mechanically, this ambiguity shows in the structure of transmon many-body spectra which generically show statistical signatures of both integrability (evidenced by Poisson statistics) and chaos (Wigner-

Dyson statistics) [3]. A transmon gate is then a driven protocol transiently exciting a subsystem of qubits close to the ones targeted by the gate operation. The faster a gate operation, the higher the chances that it connects to semiclassically unstable sectors of the state space [4]. For gates transiently populating part of the higher-lying state space, instabilities may thus become relevant already in architectures where the computational subspace itself is operated in a stability island [3]. While not necessarily reflected in the gate fidelities, the presence of such instabilities will likely impact gate implementation. It is thus imperative to clarify the role of the nonlinearity for the dynamics of coupled transmons.

Here, we show how to analyse and detect signatures of non-integrability in a universal set of transmon qubit gates. We adapt methodology from quantum nonlinear dynamics and many-body localization theory to the unitary operators $U(t)$ implementing single-qubit and two-qubit gates. These time evolutions are realized by time-dependent external fields, designed with optimal control [10] as a map on the computational state space, but transiently acting in the larger space of high-lying states. To be specific, we consider the smallest possible structure comprising two transmon qubits coupled via an intermediate cavity subject to a microwave drive [9], see Fig. 1. We find that while traces of nonlinear and even chaotic dynamics are visible in the operators implementing fast gates, they present no principal obstruction to high gate fidelities. The reason is the finite dimensionality of the effective Hilbert space subject to control. While classical chaotic time evolution is unpredictable by definition, projection onto a finite dimensional quantum Hilbert space leads to more manageable dynamics, which can be optimized towards a desired output. Crucially, however, nonlinearity correlates with a high sensitivity of gate fidelities to just very small modifications in the Hamiltonian parameters.

Model and control protocols We analyze two universal sets of gates, with Hadamard and local phase gates as representative single-qubit operations and the BGATE as entangling operation. The latter yields the smallest decomposition of an arbitrary two-qubit operation into gates of a universal set [11]. For full operability of the quantum hardware, it is im-

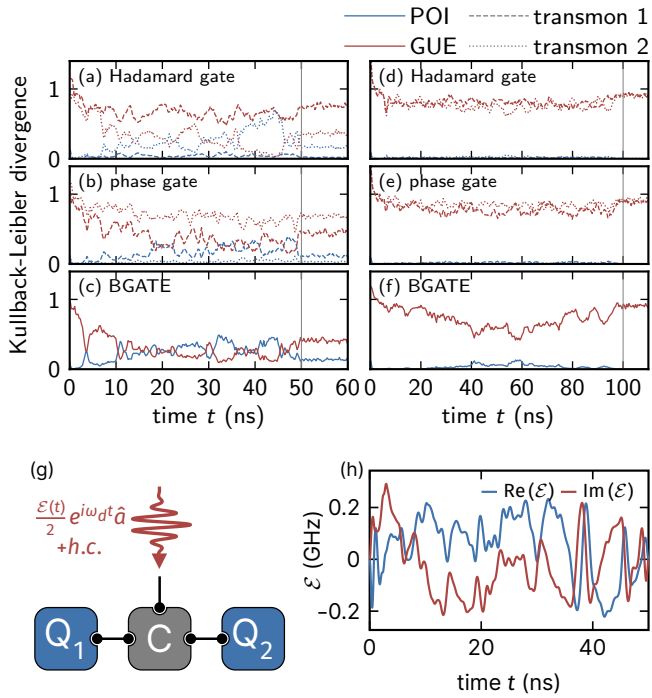


FIG. 1. **Spectral analysis of chaotic fluctuations in single-qubit and two-qubit gates** (a–f) The statistics of the relative eigenphase differences of the time evolution are compared to Poisson (POI), resp. Gaussian (GUE) statistics using the Kullback-Leibler (KL) divergence for gate durations of $T = 50$ ns (left) and $T = 100$ ns (right). Deviations from Poisson statistics are observed in panels (a), (b) and (c) and to a lesser extent in panel (f). (g) Pictorial view of two transmon qubits coupled via a joint transmission line cavity. Gates are implemented by applying a fine-tuned microwave field driving the cavity [9], shown in (h) for the fast entangling BGATE (c).

portant to inspect a complete universal set, as this requires the ability to both create and destroy entanglement. The Hamiltonian for two transmon qubits with a joint transmission line cavity subject to a microwave drive in a frame rotating with the drive frequency ω_d reads [9]

$$H(t) = \sum_{q=1}^2 \left[\delta_q b_q^\dagger b_q + \frac{\alpha_q}{2} b_q^\dagger b_q^\dagger b_q b_q + g (b_q^\dagger a + b_q a^\dagger) \right] + \delta_c a^\dagger a + \frac{1}{2} \mathcal{E}(t) a + \frac{1}{2} \mathcal{E}^*(t) a^\dagger, \quad (1)$$

where b_q and a are the annihilation operators for the q th transmon and the cavity, respectively, $\delta_q = \omega_q - \omega_d$ and $\delta_c = \omega_c - \omega_d$ are the qubit and cavity detunings from ω_d , α_q the qubit anharmonicities, and g is the qubit-cavity coupling strength. $\mathcal{E}(t)$ denotes the amplitude of the cavity drive with the time-dependency derived via gate optimization [9]. The quantum gates we analyze operate in the quasi-dispersive straddling qutrits (QuaDiSQ) regime where the cavity cannot be adiabatically eliminated and transmon levels outside the computational subspace are exploited for fast gate operation [9] (with $\dim \mathcal{H} = 150$, see the supplemental material (SM) [12] for details). The fastest possible universal set of

gates uses gate durations of $T = 50$ ns [9]. This limit is set by the local gates, whereas the fastest entangling operation, \sqrt{i} SWAP, requires only about 10 ns [9]. Fast gate operations come at the expense of complex and spectrally broad pulse shapes $\mathcal{E}(t)$, see Fig. 1(h) for an example. Increasing the gate durations by a factor of two to $T = 100$ ns significantly reduces both temporal and spectral complexity of the pulses [9].

Spectral analysis The time evolution operators $U(t)$ corresponding to the gate operations contain information about the entire dynamics up to time t , whereas the instantaneous eigenvalues of the Hamiltonian (1) capture only time-local information. We therefore analyze the statistical properties of the instantaneous eigenvalues of $U(t)$, using the Kullback-Leibler (KL) divergence [13] to quantify the deviation of their probability distribution from two limiting cases of Poisson (POI) and Gaussian (GUE) statistics for integrable, resp. chaotic, dynamics. Figure 1(a)–(f) shows the two corresponding KL divergences $D_{\text{KL}}(P_{\text{rel.}}|P_{\text{POI}})$ (see SM [12] for computational details): While $D_{\text{KL}}(P_{\text{rel.}}|P_{\text{POI}})$ vanishes almost everywhere for the slower set of gates (Fig. 1(d)–(f)), the gates at the quantum speed limit (Fig. 1(a)–(c)) show chaotic fluctuations, more closely. Panel (a) displays the eigenphases $\phi_n(t)$ of $U(t)$ as blue lines, appearing as blue areas due to their high density, and the color code showing exemplarily the evolution of the computational basis state $|00\rangle$ (where larger and darker (smaller and brighter) dots indicate a larger (smaller) overlap of the time-evolved state $|\Psi_{00}(t)\rangle = U(t)|00\rangle$ with the eigenstate $|\Phi_n(t)\rangle$ to which the blue line corresponds). Figure 2 (b) provides a blow-up of the first 5 ns of the dynamics. This time frame is interesting because it shows the transition from straight lines and line crossings for all $\phi_n(t)$ into a regime where avoided crossings between lines start to become more frequent. The emerging many-body nonlinear behavior is witnessed by the KL divergence of the eigenphases $\phi_n(t)$ in Fig. 2(c). While up to $t \approx 3$ ns, the KL divergence shows an almost perfect match with an ideal POI statistics, evidencing integrable behavior, it diverges from POI statistics and shows a larger match with GUE statistics, signalling emergent chaotic behavior, between 3 ns and 4 ns. Figure 2 (d)–(g) shows the actual distributions at four representative times, with an almost perfect match with ideal POI statistics before avoided crossings play a role (d). Similarities of $P_{\text{rel.}}$ to POI statistics also dominate just before (e) and after (g) the chaotic regime, whereas a larger (but far from perfect) match with GUE statistics is observed in (f). Interestingly, after 4 ns the dynamics becomes less chaotic again. Such emergence and disappearance of chaos occurs several times over the entire protocol and is also observed for the other fast gates with chaotic behavior in Fig. 1. Remarkably, the (re)emergence of chaotic behavior does not have any negative impact on the gate errors — these are identically small for both fast and slow protocols in Fig. 1. The optimized control field seems to navigate the computational basis states safely through the chaotic regions.

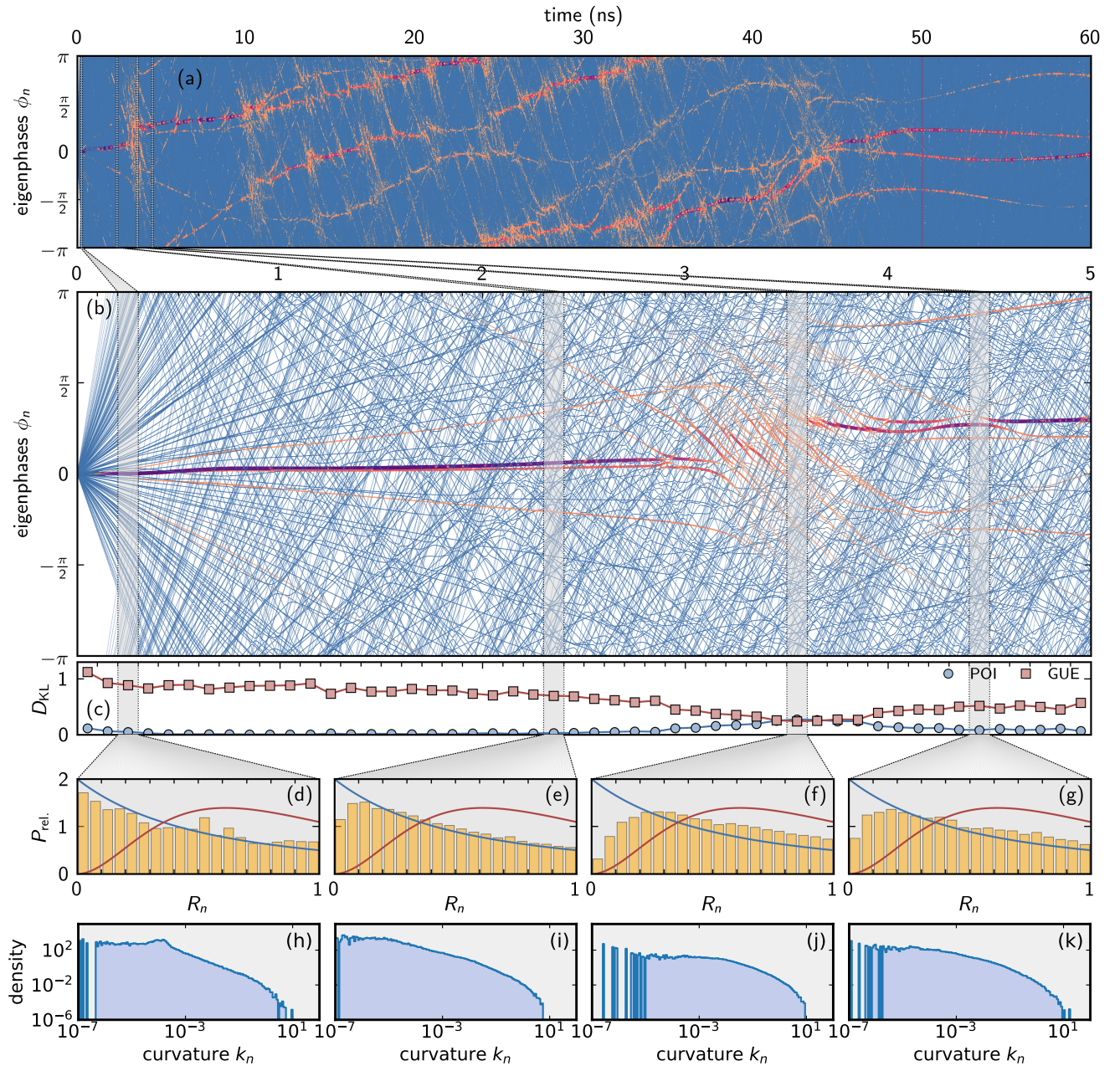


FIG. 2. **Detailed analysis of the fast entangling BGATE** (c): KL divergences as in Fig. 1(c) (red dotted line: end of pulse). (a),(b): Instantaneous eigenphases $\{\phi_n(t)\}$ of $U(t)$ (blue lines) with their population $p_i(t)$ indicated by size and color of the dots. (d)–(g): Probability distributions of the relative eigenphases in the time intervals highlighted in gray in (b), compared to ideal Poisson (blue) and Gaussian (red) distributions. (h)–(k): Dimensionless level curvatures $k_n(t)$ for the intervals analyzed in (d)–(g).

Curvature distributions Beyond the statistics of eigenphases, the structure of avoided crossings can be another indicator of nonlinear dynamics. Correlations lead to effective phase repulsion and to an overall more ‘curvy’ pattern of phase evolutions in Fig. 2 (b). To quantify this structure, we consider the curvature κ_n of the eigenphases, $\kappa_n(t) = d^2\phi_n(t)/dt^2$. In the limiting cases of localization and chaos,

they follow distinct distributions [14–16],

$$P_{\text{POI}}(k) = \frac{\mathcal{N}_{\text{POI}}}{(1+k^2)}, \quad P_{\text{GUE}}(k) = \frac{\mathcal{N}_{\text{GUE}}}{(1+k^2)^2}, \quad (2)$$

where $\mathcal{N}_{\text{POI/GUE}}$ is a normalization constant and k the curvature κ , rescaled by the average spacing Δ and the variance of the velocity distribution [15, 16], $k_n = \kappa_n \Delta(\phi_n) / (2\pi \text{Var}(\partial_t \phi_n))$. For large k , Eq. (2) gives a power-law behavior, $P(k \rightarrow \infty) \propto \|k\|^{-\tilde{\beta}}$ with $\tilde{\beta} = 2(4)$

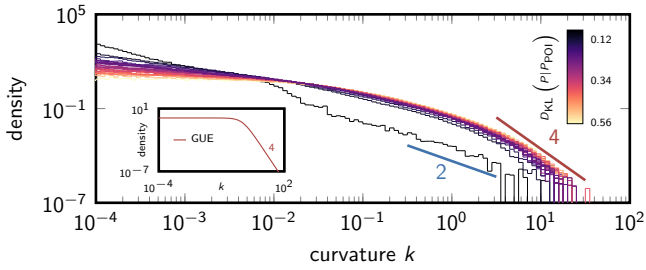


FIG. 3. **Curvature statistics** for the time evolution implementing the BGATE. The color of the curvature histogram encodes the KL divergence of the eigenphase spacing. For large curvatures, solid lines indicate polynomial fits to the data, consistent with GUE-like behavior (shown in the inset) of a power-law decay with exponent $\tilde{\beta} = 4$ for all but the very first time interval which is consistent with Poisson-like behavior and $\tilde{\beta} = 2$.

for the Poisson (GUE) case [14, 16, 17]. Analysis of the eigenphase curvatures in Fig. 2 (h)–(k) corroborates the occurrence of chaotic fluctuations indicated by the statistical analysis of the eigenphase differences: Noting the double-logarithmic scale, it is clear that small curvatures are prevalent for regular dynamics in Fig. 2 (h), (i), and, to a lesser extent (k), whereas larger curvatures have significantly more weight in the region of nonlinear behavior, cf. Fig. 2(j). To make the correspondence between the eigenphase statistics and the occurrence of nonlinear/integrable dynamics more quantitative, we calculate the curvature of the eigenphases in each of 30 equally-spaced t segments of length 0.5 ns. The resulting distributions of the curvatures are shown in Fig. 3, where the color code corresponds to the KL divergence $D(P|P_{\text{POI}})$ of the eigenphase spacing, calculated for the same time interval. Importantly, from the perspective of curvatures, there are traces of nonlinear GUE-like dynamics for all but the initial time intervals. Despite the fact that our spectrum exhibits only 150 levels, the curvature statistics show general similarity to pure GUE-behavior (see inset of Fig. 3), exhibiting a plateau of constant probabilities for small curvatures $k \lesssim 1$ followed by a crossover to polynomial decay of probabilities in the high curvature regime. While our data does not exhibit a perfectly flat plateau, it does show the more defining power-law decay for large curvatures, reproducing the GUE exponent of $\tilde{\beta} = 4$ for all but the initial time interval. The latter instead follows a POI-like behavior with exponent $\tilde{\beta} = 2$.

We thus find that statistical analysis of the curvatures reflects the presence of avoided crossings in a strikingly clear way. Importantly, it allows for the isolation of a subset of states for which the predictions of random matrix theory apply. Remarkably, this subset of states can comprise only a small portion of Hilbert space. In such cases, the KL divergence has difficulty to indicate the onset of chaotic fluctuations, due to the low weight of the affected states in the sum over all states. This difficulty affects also wave function statistics and out-of-time-ordered correlators which are not sufficiently sensitive as we show in the SM [12]. In con-

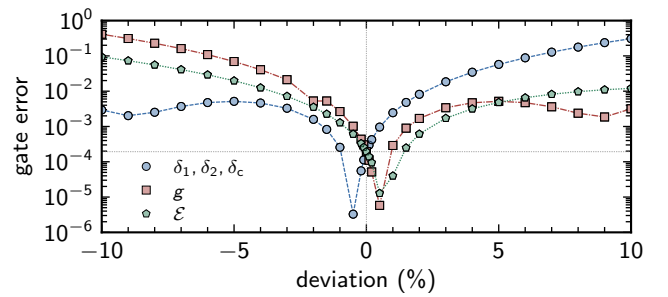


FIG. 4. **Gate error for the fast BGATE** with $T = 50$ ns as a function of deviations in the Hamiltonian parameters. The horizontal lines indicate the gate error in the absence of any deviations.

trast, “sorting” the evolutions according to their curvature allows for identifying the avoided crossings that are a defining hallmark of the chaotic fluctuations.

Robustness All gate protocols investigated here exhibit remarkably low gate errors [9], despite the complexity of their time-evolution, but the transient and recurrent regimes of instability identified above are likely to affect gate performance. For ideal protocols, the low errors are readily rationalized from the perspective of quantum optimal control: In a finite-dimensional Hilbert space, it is sufficient to know the exact Hamiltonian that governs the system’s dynamics in order to derive high-fidelity control solutions. However, the assumption of precisely knowing the Hamiltonian is not realistic. For superconducting qubits, in particular, system parameters are typically not very accurately known and moreover tend to drift over time. Similar uncertainties apply also to the control fields, due to inaccuracies in the generating hardware. Focussing on the fast BGATE protocol where signatures of chaotic behavior have been most apparent, we suspect small deviations in the Hamiltonian or the control parameters to cause large gate errors. Considering constant deviations, Fig. 4 analyzes gate robustness with respect to deviations in the transmon and cavity frequencies $\delta_1, \delta_2, \delta_c$, the coupling strength g , and the field amplitude $\mathcal{E}(t)$. We quantify robustness by the (generalized) gate error, defined in terms of the local invariants functional [18] which measures how much the entangling content of the realized gate deviates from that of the BGATE. In other words, the generalized gate error is insensitive to single-qubit rotations because these are typically easy to correct for. Despite this relaxed definition, the BGATE shows high levels of sensitivity in all considered scenarios. As soon as the deviation exceeds one per cent, the gate error is increased by two to three orders of magnitude, depending on the sign of the deviation (the asymmetry with respect to the sign is readily rationalized by the gate mechanism).

While the lack of robustness in the fast BGATE may be expected for a gate showing signatures of chaotic dynamics, it would be premature to conclude that signatures of chaos in the gate dynamics categorically hamper gate robustness. Indeed, the gates of Ref. [9] have not been optimized to be robust against parameter fluctuations, and for another two-element

model system where chaotic behavior has also been observed, the situation was found to be controllable [19]. It will be interesting to find out under which conditions robust fast gates can be defined nonetheless, or whether optimization may identify protocols avoiding the emergence of strong fluctuations in the spectra and states of $U(t)$.

Conclusions We have found that fast transmon gates display clear signatures of emergent chaos. Analysis of the eigenphase curvatures has turned out to be the most sensitive tool to diagnose signatures of non-integrability, due to the ability to identify the subset of states evolving through avoided crossings. More conventional measures, such as the KL divergence of the time evolution eigenphases or measures based on population dynamics, are hampered by an indiscriminate average over state space. For gates that display chaotic fluctuations, time intervals where the statistics have a much larger match with the chaotic limit are followed by time intervals where integrable statistics are recovered. This suggests that the optimized pulses are able to steer the dynamics during a chaotic sea without compromising the gate fidelity. However, when allowing for variations in the parameters characterizing the Hamiltonian, the gate error increases by orders of magnitude already for small deviations. We have thus shown that dynamical instabilities arising from the transmon nonlinearity adversely affect gate implementations already for two qubits and a coupler.

One may wonder whether there is a simple connection between robustness and signatures of chaos. The answer to this question is less obvious than one might conjecture at first glance. The quantum speed limit, for instance, does not impede implementation of energy-efficient quantum gates [20]. Possibly, energy-efficient quantum gates at the speed limit would be less prone to chaotic fluctuations than the gates analyzed here. Such gates can be derived by repeating the gate optimization of Ref. [9], including energy efficiency as an additional time-dependent constraint [21] or explicitly enforcing robustness, e.g. with ensemble optimization [22] or by accounting for the parameter fluctuations in the optimization functional [23] or equations of motion [24]. Generally, robustness of quantum control is key to implementing quantum protocols in real physical systems [10, 25]. Transmon architectures represent a particularly challenging use case, and future work will have to show whether the adverse effects of the transmon nonlinearity can be tamed to harness its benefits for quantum advantage.

We thank David DiVincenzo for fruitful discussions. Financial support from the Deutsche Forschungsgemeinschaft (DFG), Project No. 277101999, CRC 183 (project C05), and the Cluster of Excellence Matter and Light for Quantum Computing (ML4Q) EXC 2004/1 – 390534769 is gratefully acknowledged.

DATA AVAILABILITY

The details of the optimized gate protocols and the numerical data shown in the figures are available on Zenodo [26].

Supplemental material to “Chaotic fluctuations in a universal set of transmon qubit gates”

Daniel Basilewitsch,¹ Simon-Dominik Börner,² Christoph Berke,²
Alexander Altland,² Simon Trebst,² and Christiane P. Koch^{1,*}

¹*Dahlem Center for Complex Quantum Systems and Fachbereich Physik, Freie Universität Berlin, D-14195 Berlin, Germany*

²*Institute for Theoretical Physics, University of Cologne, D-50937 Cologne, Germany*

(Dated: January 24, 2024)

MODEL AND SYSTEM PARAMETERS

The Hilbert space is constructed as the tensor product of the Hilbert spaces of the two transmons and the cavity. Taking the local Hilbert space dimensions to be 5 for each of the transmons and 6 for the cavity, resulted in a total Hilbert space dimension $N = 150$, sufficient for numerical convergence. The computational states $|00\rangle, |01\rangle, |10\rangle, |11\rangle$ are the *dressed* basis states, i.e., the eigenstates of H in the absence of the control which do not change further once the gate protocol is finished. In detail, $|i_1 i_2\rangle$ refers to the eigenstate of H , cf. Eq. (1) in the main text, with $\mathcal{E}(t) = 0$, which has with the largest overlap with the bare Fock state $|i_1\rangle \otimes |i_2\rangle \otimes |i_c = 0\rangle = |i_1, i_2, 0\rangle_{\text{Fock}}$, where i_1, i_2 and i_c label excitations of the two transmons and the cavity.

Table I provides an overview of all relevant parameters.

TABLE I. Parameters for the system illustrated in Fig. 1(a) of the main text, consisting of two transmons, Q_1 and Q_2 , and a cavity C . Taken from Ref. [9].

frequency cavity C	$\omega_c/2\pi$	6.2 GHz
base frequency transmon Q_1	$\omega_1/2\pi$	6.0 GHz
base frequency transmon Q_2	$\omega_2/2\pi$	5.9 GHz
anharmonicity transmon Q_1	$\alpha_1/2\pi$	-290 MHz
anharmonicity transmon Q_2	$\alpha_2/2\pi$	-310 MHz
coupling between transmons and cavity	$g/2\pi$	70 MHz
driving frequency of cavity C	$\omega_d/2\pi$	5.93 GHz

KULLBACK-LEIBLER DIVERGENCE OF THE TIME EVOLUTION EIGENPHASES

The instantaneous eigenvalues of the time evolution $U(t)$ corresponding to the gate implementation are denoted by $\lambda_1(t), \dots, \lambda_N(t) \in \mathbb{C}$, which have a unique representation, $\lambda_n(t) = e^{i\phi_n(t)}$, $n = 1, \dots, N$, in terms of eigenphases, $\phi_1(t), \dots, \phi_N(t) \in [-\pi, \pi)$. Assuming without loss of generality $\phi_1(t) \leq \phi_2(t) \leq \dots \leq \phi_N(t)$ for every time t [27], we define nearest neighbor differences as $\Delta\phi_n(t) \equiv \phi_{n+1}(t) - \phi_n(t)$, $n = 1, \dots, N - 1$. The corresponding relative differences are then given as [28]

$$r_n(t) = \frac{\Delta\phi_n(t)}{\Delta\phi_{n+1}(t)}, \quad R_n(t) = \min \left\{ r_n(t), \frac{1}{r_n(t)} \right\} \quad (\text{S3})$$

with $n = 1, \dots, N - 2$ and $R_n(t) \in [0, 1]$ which is convenient for statistical analysis. In the limiting cases of integrable, resp. chaotic dynamics, the $\{R_n(t)\}$ are expected to obey Poissonian, respectively Wigner-Dyson statistics. Up to inessential corrections [29], the corresponding distributions are given by [30]

$$P_{\text{POI}}(R) = \frac{2}{(1+R)^2}, \quad (\text{S4a})$$

$$P_{\text{GUE}}(R) = \frac{162\sqrt{3}}{4\pi} \frac{(R+R^2)^2}{(1+R+R^2)^4}. \quad (\text{S4b})$$

Deviations from the limiting cases P_{POI} or P_{GUE} can be quantified using the Kullback-Leibler (KL) divergence, in analogy to the spectral analysis of the static qubit arrays [3]. More precisely, when comparing to Poisson (POI) statistics, a non-zero KL divergence signals the emergence of statistical correlations. Conversely, chaotic fluctuations are indicated by the KL divergence with respect to P_{GUE} approaching zero. For two statistical distributions P_1 and P_2 , their KL divergence is given by [13]

$$D_{\text{KL}}(P_1|P_2) = \sum_{R \in \mathcal{R}} P_1(R) \log \left(\frac{P_1(R)}{P_2(R)} \right), \quad (\text{S5})$$

where P_1 and P_2 are normalized such that $\sum_{R \in \mathcal{R}} P_1(R) = \sum_{R \in \mathcal{R}} P_2(R) = 1$. Since in general $D_{\text{KL}}(P_1|P_2) \neq D_{\text{KL}}(P_2|P_1)$, we normalize the KL divergences individually such that $D_{\text{KL}}(P_{\text{GUE}}|P_{\text{POI}}) = 1$ and $D_{\text{KL}}(P_{\text{POI}}|P_{\text{GUE}}) = 1$ which ensures $0 \leq D_{\text{KL}}(P_{\text{rel.}}|P_{\text{POI}}), D_{\text{KL}}(P_{\text{rel.}}|P_{\text{GUE}}) \leq 1$.

To gather enough statistical data, we divide the entire time span into 250 intervals and collect all R_n values from a fixed interval, yielding a single, joint distribution $P_{\text{rel.}}^{\text{joint}}$ for each interval. For these joint distributions, the Kullback-Leibler divergences are calculated and displayed in Fig. 1(a–f) of the main text at the respective interval midpoint.

FURTHER OBSERVABLES

For completeness we present here our findings using analysis of wavefunction statistics and out-of-time-ordered correlators.

Occupation dynamics

In order to analyse the dynamics of the states rather than the time-dependent spectra, we introduce and discuss several measures that are based on the population dynamics and show which of those are sensitive regarding the observed non-integrability of the dynamics.

As a first step, we consider the time occupation of the time-evolved computational basis states $|00\rangle, |01\rangle, |10\rangle, |11\rangle$. The question is whether traces of the non-integrability we observed in the time-dependent spectra are visible in the occupation of computational states. Figure S5 (a) shows that this is not the case. Tracing the occupation of a state initialized as $|00\rangle$ over the first 5 ns — an interval which we saw contains regions of regular and non-integrability in the window between 3 ns to 4 ns — we observe no signatures of irregularity in the occupation of states.

The occupation of single particle states close to the ground state thus does not respond to transient instabilities in the system. We may therefore rule out the plain occupation dynamics as a good indicator of non-integrability. However, one may speculate that the occupation of higher lying states may be a more sensitive indicator. A first question to be asked is how much of the total spectral weight carried by an evolving state actually lies outside the logical subspace. To answer it, we

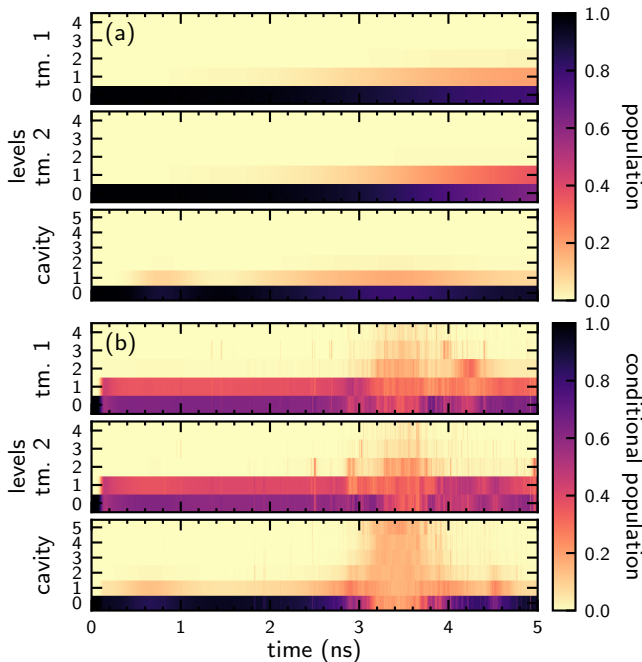


FIG. S5. **Occupation dynamics.** (a) Occupation dynamics for $|\Psi(t)\rangle = U(t)|00\rangle$ during the first 5 ns of the BGATE. The three panels show the instantaneous, bare level occupations for $\rho_{1/2/c}(t) = \text{tr}_{2,c/1,c/1,2}\{|\Psi(t)\rangle\langle\Psi(t)|\}$ of the two transmons (with five levels per transmon) and the cavity (with six levels), respectively. (b) The conditional population dynamics, cf. Eq. (S9), for the same state.

define

$$p_{\text{sub}}(t) = \frac{1}{4} \sum_{\{|\Psi_{\text{in}}\rangle\}} \langle\Psi_{\text{in}}|U^\dagger(t)\Pi_{\text{sub}}U(t)|\Psi_{\text{in}}\rangle,$$

$$\Pi_{\text{sub}} = \sum_{\{|\Psi_{\text{in}}\rangle\}} |\Psi_{\text{in}}\rangle\langle\Psi_{\text{in}}|,$$

where $|\Psi_{\text{in}}\rangle \in \{|00\rangle, |01\rangle, |10\rangle, |11\rangle\}$. Here, Π_{sub} is the projector onto the logical subspace and p_{sub} the time dependent probability that a state initialized as a computational state stays inside this space.

The fast gates analyzed in Fig. 1(a-c) of the main text are characterized for a comparatively large amount of population outside of the logical subspace at intermediate times [9]. For the BGATE, for example, this figure hovers around 10-20% at most times, without noticeable changes during the irregular time window. We conclude that the cumulative weight sitting in the non-computational state likewise is blind to dynamical instability. We thus zoom in to the next level of resolution and monitor the occupation of individual “many-body” eigenstates $\Phi_n(t)$ of the full evolution operator $U(t)$. With an initial state as before, $|\Psi_{\text{in}}\rangle \in \{|00\rangle, |01\rangle, |10\rangle, |11\rangle\}$, we define the probabilities

$$p_n(t) = |\langle\Phi_n(t)|U(t)|\Psi_{\text{in}}\rangle|^2, \quad (\text{S6})$$

normalized as $\sum_n p_n = 1$. The color coding in Fig. 2(a) and (b) of the main text shows the distribution of these weights over the eigenphases ϕ_n of the first 150 states of the system. In this representation, blue color is used to indicate the bare eigenphases, while a combined color coding from dark purple to light orange and dot size coding from larger to smaller dots indicates larger to smaller state occupation. This visual data indeed shows a massive fragmentation of the evolving state over a high dimensional subspace during intervals where the spectral analysis flags non-integrability (via the KL divergence). Outside these regions, the spectral weight remains concentrated on a few states in and outside the computational subspace. However, while the correlation of state fragmentation and non-integrability is a generic phenomenon, we have also observed milder forms of transient state spreading in gate protocols without chaotic instabilities, such as the slower operations shown in Fig. 1(d)–(f) of the main text.

While the above data may serve as a visual indicator for dynamical signatures of non-integrability, it contains too much information to be quantitatively useful. The simplest way to condense it is to track the time dependent fraction M/N of the number of levels, M , whose occupation probability exceeds a given threshold p :

$$P_p(t) = \frac{1}{N} \sum_{n=1}^N \Theta(p_n(t) - p), \quad (\text{S7})$$

where Θ is the Heaviside step function. Taking $p = 1\%$, $P_p(t)$ reflects the spreading/contracting of the colored dots in Fig. 2(a) of the main text. Inspecting this figure is, however,

also relatively non-expressive in that it is qualitatively similar to the total occupation of the out-of-computational subspace $1 - P_{\text{sub}}$, hinting at a limited usefulness of Eq. (S7).

A more meaningful quantity is obtained by the projection of exact instantaneous eigenstates Φ_n onto select occupation eigenstates, $|i_1, i_2, i_c\rangle_{\text{Fock}}$, weighted with the occupation probabilities p_n computed according to Eq. (S6),

$$P_{i_1, i_2, i_c}(t) = \sum_n p_n(t) |\langle \Phi_n(t) | i_1, i_2, i_c \rangle_{\text{Fock}}|^2, \quad (\text{S8})$$

Note that Eq. (S8) is quartic in the states $\{|\Phi_n(t)\rangle\}$. (A squared amplitude is hiding in p_n .) We read these fourth moments of wave functions as a sum over conditional probabilities, where the first factor p_n states the representation of state Φ_n in the actual time evolved initial state, and the second its probability to be found in the Fock space state $|i_1, i_2, i_c\rangle_{\text{Fock}}$. These quantities can be further reduced to yield, say, the representation of the first transmon's states as

$$P_{i_1}(t) = \sum_{i_2=0}^{N_2-1} \sum_{i_c=0}^{N_c-1} P_{i_1, i_2, i_c}(t), \quad (\text{S9})$$

Fig. S5 (b) shows how this data efficiently detects the instability in the high lying sector of Hilbert space during the interval between 3 and 4 ns. In this way, it represents a good compromise between the bare occupation probabilities of the low lying states, which are blind to the presence of unstable regimes (Fig. S5 (b)), and the excessive data carried by the full set of amplitudes $\{\Phi_n\}$.

To summarize, we have found two state population-based measures, Eqs. (S6) and (S9), that are sensitive to the non-integrability of the dynamics. Unfortunately, both of them require the diagonalization of $U(t)$ and their computation will therefore become difficult for larger systems. In contrast, the analyses based solely upon the occupation dynamics, i.e., both level or subspace occupations, show no correlation with the observed irregularities. This suggests that such irregularities might be easily overseen if only the occupation dynamics is analyzed.

OUT-OF-TIME-ORDERED CORRELATORS (OTOCs)

Additionally, we check so-called out-of-time-ordered correlators (OTOCs), which are a good measure for information scrambling as well as quantum chaos [31]. Let V and W be two Hermitian operators, the OTOC is given by

$$F(t) = \Re \{ \langle W^\dagger(t) V^\dagger W(t) V \rangle_\Psi \}, \quad W(t) = U^\dagger(t) W U(t), \quad (\text{S10})$$

which depends on the state $|\Psi\rangle$ for which it is evaluated. If V and W are also unitary, besides being Hermitian, and fulfill $[V, W] = 0$, we have $F(0) = 1$ for all $|\Psi\rangle$ and a deviation like $F(t) < 1$ at later times t indicates information scrambling between the two subspaces acted upon by V and

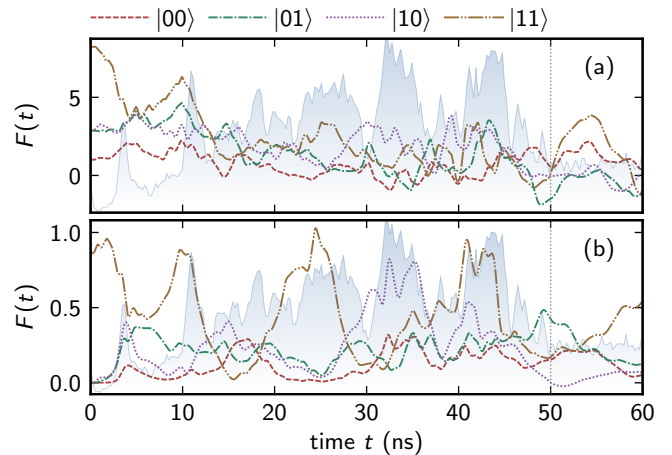


FIG. S6. **OTOCs for the fast BGATE** with $T = 50$ ns. The operators are (a) $V = b_1 + b_1^\dagger$ and $W = b_2 + b_2^\dagger$ as well as (b) $V = b_1^\dagger b_1$ and $W = b_2^\dagger b_2$. The blue area in the background indicates the KL divergence for the POI statistics from Fig. 1 (e) of the main text in arbitrary units.

W . While in two-level systems a possible choice would be $V, W \in \{\sigma_x, \sigma_y, \sigma_z\}$ such that V and W are both Hermitian *and* unitary. Unfortunately, this is not possible in our case due to the larger Hilbert space. However, since unitarity of V and W is not a requirement, we choose

$$V = b_1 + b_1^\dagger, \quad W = b_2 + b_2^\dagger \quad (\text{S11a})$$

and

$$V = b_1^\dagger b_1, \quad W = b_2^\dagger b_2. \quad (\text{S11b})$$

Figure S6 shows the OTOCs for those two choices of W and V for all four computational basis states $|00\rangle, |01\rangle, |10\rangle, |11\rangle$ for the fast BGATE. The blue background area indicates the KL divergence with respect to the POI statistics in order to compare the course of the OTOCs to peaks in the KL divergence indicating chaotic regions. We find the OTOCs to not match the KL divergence, neither for the two choices of V and W presented in Fig. S6 nor for other choices.

* christiane.koch@fu-berlin.de

- [1] P. Krantz, M. Kjaergaard, F. Yan, T. P. Orlando, S. Gustavsson, and W. D. Oliver, A quantum engineer's guide to superconducting qubits, *Applied Physics Reviews* **6** (2019).
- [2] J. J. García-Ripoll, *Quantum Information and Quantum Optics with Superconducting Circuits* (Cambridge University Press, 2022).
- [3] C. Berke, E. Varvelis, S. Trebst, A. Altland, and D. P. DiVincenzo, Transmon platform for quantum computing challenged by chaotic fluctuations, *Nat. Commun.* **13**, 2495 (2022).
- [4] J. Cohen, A. Petrescu, R. Shillito, and A. Blais, Reminiscence of Classical Chaos in Driven Transmons, *PRX Quantum* **4**, 020312 (2023).

- [5] S.-D. Börner, C. Berke, D. P. DiVincenzo, S. Trebst, and A. Altland, Classical Chaos in Quantum Computers (2023), [arXiv:2304.14435](https://arxiv.org/abs/2304.14435).
- [6] F. W. Strauch, P. R. Johnson, A. J. Dragt, C. J. Lobb, J. R. Anderson, and F. C. Wellstood, Quantum Logic Gates for Coupled Superconducting Phase Qubits, *Phys. Rev. Lett.* **91**, 167005 (2003).
- [7] P. Magnard, P. Kurpiers, B. Royer, T. Walter, J.-C. Besse, S. Gasparinetti, M. Pechal, J. Heinsoo, S. Storz, A. Blais, and A. Wallraff, Fast and Unconditional All-Microwave Reset of a Superconducting Qubit, *Phys. Rev. Lett.* **121**, 060502 (2018).
- [8] S. Deffner and S. Campbell, Quantum speed limits: from Heisenberg’s uncertainty principle to optimal quantum control, *J. Phys. A: Math. Theor.* **50**, 453001 (2017).
- [9] M. H. Goerz, F. Motzoi, K. B. Whaley, and C. P. Koch, Charting the circuit QED design landscape using optimal control theory, *npj Quantum Inf.* **3**, 37 (2017).
- [10] C. P. Koch, U. Boscain, T. Calarco, G. Dirr, S. Filipp, S. J. Glaser, R. Kosloff, S. Montangero, T. Schulte-Herbrüggen, D. Sugny, and F. K. Wilhelm, Quantum optimal control in quantum technologies. strategic report on current status, visions and goals for research in europe, *EPJ Quantum Technol.* **9**, 19 (2022), 2205.12110.
- [11] J. Zhang, J. Vala, S. Sastry, and K. B. Whaley, Minimum Construction of Two-Qubit Quantum Operations, *Phys. Rev. Lett.* **93**, 020502 (2004).
- [12] Supplemental material.
- [13] S. Kullback and R. A. Leibler, On Information and Sufficiency, *Ann. Math. Stat.* **22**, 79 (1951).
- [14] M. Filippone, P. W. Brouwer, J. Eisert, and F. von Oppen, Drude weight fluctuations in many-body localized systems, *Phys. Rev. B* **94**, 201112 (2016).
- [15] F. von Oppen, Exact distribution of eigenvalue curvatures of chaotic quantum systems, *Phys. Rev. Lett.* **73**, 798 (1994).
- [16] A. Maksymov, P. Sierant, and J. Zakrzewski, Energy level dynamics across the many-body localization transition, *Phys. Rev. B* **99**, 224202 (2019).
- [17] S. J. Garratt, S. Roy, and J. T. Chalker, Local resonances and parametric level dynamics in the many-body localized phase, *Phys. Rev. B* **104**, 184203 (2021).
- [18] M. M. Müller, D. M. Reich, M. Murphy, H. Yuan, J. Vala, K. B. Whaley, T. Calarco, and C. P. Koch, Optimizing entangling quantum gates for physical systems, *Phys. Rev. A* **84**, 042315 (2011).
- [19] A. V. Andreev, A. G. Balanov, T. M. Fromhold, M. T. Greenaway, A. E. Hramov, W. Li, V. V. Makarov, and A. M. Zagoskin, Emergence and control of complex behaviors in driven systems of interacting qubits with dissipation, *npj Quantum Inf.* **7**, 1 (2021).
- [20] M. Aifer and S. Deffner, From quantum speed limits to energy-efficient quantum gates, *New J. Phys.* **24**, 055002 (2022).
- [21] J. P. Palao, D. M. Reich, and C. P. Koch, Steering the optimization pathway in the control landscape using constraints, *Phys. Rev. A* **88**, 053409 (2013).
- [22] M. H. Goerz, E. J. Halperin, J. M. Aytac, C. P. Koch, and K. B. Whaley, Robustness of high-fidelity Rydberg gates with single-site addressability, *Phys. Rev. A* **90**, 032329 (2014).
- [23] A. Koswara, V. Bhutoria, and R. Chakrabarti, Robust control of quantum dynamics under input and parameter uncertainty, *Phys. Rev. A* **104**, 053118 (2021).
- [24] T. Araki, F. Nori, and C. Gneiting, Robust quantum control with disorder-dressed evolution, *Phys. Rev. A* **107**, 032609 (2023).
- [25] C. A. Weidner, E. A. Reed, J. Monroe, B. Sheller, S. O’Neil, E. Maas, E. A. Jonckheere, F. C. Langbein, and S. G. Schirmer, Robust quantum control in closed and open systems: Theory and practice (2023), [arXiv:2401.00294 \[quant-ph\]](https://arxiv.org/abs/2401.00294).
- [26] D. Basilewitsch, S.-D. Börner, C. Berke, A. Altland, S. Trebst, and C. P. Koch, Data underpinning ‘Chaotic fluctuations in a universal set of transmon qubit gates’, [10.5281/zenodo.10160591](https://arxiv.org/abs/2305.10160) (2023).
- [27] Note that this sorting might break continuity if a single eigenphase $\phi_n(t)$ is viewed as a function of time.
- [28] V. Oganesyan and D. A. Huse, Localization of interacting fermions at high temperature, *Phys. Rev. B* **75**, 155111 (2007).
- [29] Strictly speaking, the distribution of maximally chaotic unitary operators is governed by the circular ensembles [32]. However, where the statistics of nearby levels is concerned, this point does not matter.
- [30] Y. Y. Atas, E. Bogomolny, O. Giraud, and G. Roux, Distribution of the Ratio of Consecutive Level Spacings in Random Matrix Ensembles, *Phys. Rev. Lett.* **110**, 084101 (2013).
- [31] B. Swingle, Unscrambling the physics of out-of-time-order correlators, *Nat. Phys.* **14**, 988 (2018).
- [32] T. Guhr, A. Müller-Groeling, and H. A. Weidenmüller, Random-matrix theories in quantum physics: common concepts, *Physics Reports* **299**, 189 (1998).